Applied Catalysis B: Environmental 142–143 (2013) 494–503

Contents lists available at SciVerse ScienceDirect

Applied Catalysis B: Environmental

journal homepage: www.elsevier.com/locate/apcatb

Self-assembled graphene oxide with organo-building blocks of Fe-aminoclay for heterogeneous Fenton-like reaction at near-neutral pH: A batch experiment

Young-Chul Lee[a], Sung-Jin Chang[b], Moon-Hee Choi[c], Tae-Joon Jeon[a], Taegong Ryu[d,*], Yun Suk Huh[a,**]

[a] Department of Biological Engineering, College of Engineering, Inha University, Incheon 402-751, Republic of Korea
[b] Division of Materials Science, Korea Basic Science Institute, Daejeon 305-333, Republic of Korea
[c] Department of Beauty and Cosmetology, Graduate School of Industry, Chosun University, Gwangju 501-759, Republic of Korea
[d] Rare Metals Research Center, Korea Institute of Geoscience & Mineral Resources, Daejeon 305-350, Republic of Korea

ARTICLE INFO

Article history:
Received 5 March 2013
Received in revised form 10 May 2013
Accepted 26 May 2013
Available online 31 May 2013

Keywords:
Graphene oxide (GO)
Fe-aminoclay
Self-assembly
Fenton-like reaction
Neutral pH

ABSTRACT

Respective water-soluble graphene oxide (GO) and Fe-aminoclay were investigated for decoloration of recalcitrant organic dyes with different charges in the presence of hydrogen peroxide (H_2O_2). This oxidation process was updated in order to enable development of heterogeneous catalysts by self-assembled (precipitated) GO with organo-building blocks of Fe-aminoclay in aqueous solution. Due to electrostatic attraction between the negatively charged GO and the positively charged Fe-aminoclay, the obtained catalysts decomposed H_2O_2 at pH 6.0 to generate •OH radicals capable of breaking aromatic carbon structures. These novel catalysts were tested for cationic methylene blue (MB) and anionic orange II (OII) as model pollutants. At 1.0 wt% of H_2O_2 treatment, the apparent rate constants of MB and OII by the optimal loading of catalyst (0.61 mg/mL) were 0.35288 h^{-1} ($r^2 = 0.9721$) and 0.57930 ($r^2 = 0.9581$), respectively. Furthermore, in the two-dye mixture system, simultaneous decoloration of both dyes, to near-complete ~100% removal, was achieved after 5 h. Thus, it can be concluded that our developed catalysts for heterogeneous Fenton-like reaction at neutral pH are suitable for practical application.

1. Introduction

Self-assembly is a fascinating protocol not only in novel designs of unique nanoparticles and (nano)objects [1,2] but also in nature-inspired fabrication technologies [3–5]. The main driving force behind the self-assembly process is induced by secondary interactions involving (mainly) electrostatic attraction, hydrophobic interaction, hydrogen bonding, and van der Waals force [6]. A variety of engineered nanoparticle syntheses in recent nanotechnology studies have focused on size, shape, the ratio of surface area to volume, and surface modification chemistry in order to impart suitable functionalities to target materials in biomedical [7,8] and environmental [9] applications.

In this vein, organo-building blocks of nanomaterials of oppositely charged surfaces in aqueous solution are being utilized as precursors for construction of new architectures [4,5,10,11]. For example, water-soluble graphene oxide (GO) sheets, which is well-known to 2D carbon structures with wrinkled nanometer to micrometer scales and further used to prepare hydrophobic and conductive recovered, i.e., reduced graphene oxide (rGO) by hydrazine reducing agent in solution chemistry [12,13]. In particular, GO sheets have been often explored as substrates to decorate such nanoparticles (TiO_2, Fe_3O_4, quantum dots, and so on) [13,14]. The high-negative-charge GO surface has obliged researchers to find superior adsorbents of heavy metals [14,15] and pollutant organics [16,17]. In order to recycle GO from aqueous solution, the immobilization of GO onto macroscale matrices remains necessary. In particular, the intrinsic property of GO or magnetite as peroxidase-like activity has a significant attention after 2005 [18,19]. Recently GO has been proved the stressed induced toxicity [20] and magnetite with H_2O_2 also generated •OH radical to remove phenol compound [21]. In detail, it was found that such carbon materials or inorganic nanoparticles could decompose H_2O_2 to generate free radicals that can decolorize colorimetric dye or change it to other colors to facilitate naked-eye detection, even within wide pH and working temperate ranges [7]. GO's high functional groups with oxygen-containing hydroxyl, carbonyl, and epoxyl groups, can mimic the peroxidase enzyme to overcome the disadvantageous

* Corresponding author. Tel.: +82 42 868 3504; fax: +82 42 868 3415.
** Corresponding author. Tel.: +82 42 865 3613; fax: +82 42 865 3610.
E-mail addresses: tgryu@kigam.re.kr (T. Ryu), yunsuk.huh@inha.ac.kr, yunsuk.huh0311@gmail.com (Y.S. Huh).

0926-3373/$ – see front matter © 2013 Elsevier B.V. All rights reserved.
http://dx.doi.org/10.1016/j.apcatb.2013.05.066

sensitivity of proteins to both pH and temperature. This reaction also is associated with the Fenton-like reactions wherein Fe^{3+} or iron-sourced metal oxides form •OH radicals in the presence of H_2O_2, i.e., Fenton-like reaction catalyzes H_2O_2 by ferric iron ($Fe^{3+} + H_2O_2 \rightarrow {}^{\bullet}OOH + H^+ + Fe^{2+}$) in which the generated ferrous iron is recycled, subsequently following Fenton reaction [22–25]. The result, in any case, is that free radicals can treat recalcitrant organic contaminants in water and wastewater systems. However, the environmental applications of GO are still in their infancy.

Over a few years, Lee et al. have used water-solubilized positively charged Fe-aminoclay of ~100 nm average hydrodynamic diameter as a peroxidase-like enzyme [26], where the mechanism of action is similar to a neutral-pH Fenton-like reaction that similarly produces •OH radicals [27]. To date, the utilization of such aminoclay families has focused on self-assembled bio-inorganic composites such as DNA, protein, and enzymes with which to wrap such biomolecules with negative charges by protonated organo-building blocks of aminoclays under ambient conditions [28]. A number of trials have applied aminoclays as soil-flushing agents to the treatment of heavy metals [9] and toxic organic dyes [29], following the adsorption/desorption method. More recently, aminoclay use has been expanded to the synthesis of cationic metals such as Mn, Fe, and Ce in order to offer unique metal characteristics, beyond conventional Mg and Ca [30,31]. However, the issue of H_2O_2 decomposition by organo-building blocks of aminoclays for degradation of organic matter remains a challenge in the field of environmental engineering.

In the present study, we demonstrated flocculation of self-assembled GO with organo-building blocks of Fe-aminoclay in aqueous solution as a precipitate for a heterogeneous Fenton-like reaction. The heterogeneous reaction is advantage because of a working system in two phases where catalysts are solid to easily be recovered usually. In contrast, the homogeneous reaction is working in one phase system as ion typed catalysts present, resulting in a difficulty to recover the catalysts used [25]. As-prepared composites were tested as catalysts in a heterogeneous Fenton-like reaction modeled by the degradation of cationic and anionic dyes (methylene blue (MB) and orange II dye (OII) respectively), carried out in a batch mode at near-neutral pH. The meaningful advantages of the oxidation process under the neutral-pH condition in water and wastewater treatment processes are no need of additional pH adjustments before and after treatment as well as no generation of sludge by-products [32–38].

2. Materials and methods

2.1. Materials

All chemicals were used as received without further purification. Graphite powder (<20 μm), potassium permanganate ($KMnO_4$, ≥99.0%), potassium persulfate ($K_2S_2O_8$, ≥99.0%), phosphorus pentoxide (P_2O_5, ≥98.5%), sulfuric acid (H_2SO_4, 95.0–98.0%), iron (III) chloride hexahydrate ($FeCl_3{\cdot}6H_2O$, 270.3 g/mol, ≥97%), 3-aminopropyltriethoxysilane (≥98%, 221.37 g/mol, denoted APTES), methylene blue (319.85 g/mol, denoted MB) as a positive-model organic compound, orange II (350.32 g/mol, denoted OII) as a negative-model organic compound, 5,5-dimethylpyrroline-*N*-oxide (DMPO), and titanium (IV) oxysulfate (99.9% metals basis, ca. 15 wt% solution in dilute sulfuric acid) were purchased from Sigma–Aldrich (St. Louis, MO, USA). Dulbecco's phosphate-buffered saline (10× 1 L, Life Technologies Corp., UK) was used to PBS buffer (10 mM, pH 7.2). Bulk ethanol (18 L, 95%) was obtained from Samchun Pure Chemicals (Pyungtack City, Kyungki do, Korea). Hydrogen peroxide (H_2O_2, 34.01 g/mol, 35%) was acquired from Junsei Chemical Co., Ltd. (Tokyo, Japan). All solutions were used with Milli-Q water from a Millipore system (18 MΩ, denoted DI water).

2.2. Preparation of each graphene oxide (GO) and Fe-aminoclay

Preparatory to the synthesis of GO nanosheets, GO was prepared following the modified Hummers method [39,40]. Initially, graphite oxide was prepared prior to exfoliation, enabling GO suspensions by probe-sonication assistance. The mixture consisted of ~1 g of graphite powder, H_2SO_4 (10 mL), $K_2S_2O_8$ (2 g), and P_2O_4 (2 g), stirred at 85 °C for ~5 h with a magnetic bar. The graphite powder was oxidized, and the suspension solution was cooled with diluted DI water for 12 h. The precipitate product was filtered, washed, and dried at room temperature in a vacuum oven. Then, the as-prepared products were mixed with H_2SO_4 solution, which was cooled in an ice-water bath. This viscous liquid-type solution was added to $KMnO_4$ (10 g) and stirred in an ice-water bath for 1 h. The obtained materials subsequently were added to a prepared H_2O_2 solution (30%), the color of which was changed to bright yellow with gas bubbling. After treatment with 10 wt% HCl solution for removal of metal impurities, DI-water washing processes and filtering were performed. The graphite oxide was diluted with DI water and immediately treated with dialysis for 7 days until the pH was neutral. Finally, the purified graphite oxide powder was probe-sonicated in the 5 s on/5 s off pulse mode for 10 min (VCX 750; power: 750 W, frequency: 20 kHz; Sonics & Materials, Inc., Newtown, CT, USA) for full exfoliation, thereby affording GO.

Fe-aminoclay synthesis followed the process outlined in the literature [26–31]. Briefly, after fully dissolving 10.8 g (~0.04 mol) of $FeCl_3{\cdot}6H_2O$ in a 500-mL beaker containing 200 mL of ethanol solvent by magnetic stirring for 20 min, 13 mL (~0.06 mol) of APTES was drop-wise added to ferric-iron ethanolic solution in order to become ~0.667, i.e., the molar ratio between $FeCl_3{\cdot}6H_2O$ and APTES. After ~5 min passed, brown slurry was produced as a precipitate. The synthesized product was centrifuged at 6000 × *g* for 15 min and subsequently washed twice with 200 mL of pure ethanol to produce collection of Fe-aminoclay slurry. It was dried by ethanol evaporation at 50 °C for 24 h in an oven. Preparatory to its use, the Fe-aminoclay was crushed and powdered using a mortar and pestle. Injection of this Fe-aminoclay powder into DI water produced a Fe-aminoclay stock solution that, after solubilization by induction of full delamination of Fe-aminoclay overnight, was ready for experimental use.

2.3. Protocol of self-assembled catalysts (i.e., flocculated composites) for Fenton-like reaction

In order to construct heterogeneous H_2O_2 decomposition catalysts, each GO solution and Fe-aminoclay stock solution was mixed to the ratio of 2 mL:6 mL (denoted as Sample #01), 4 mL:4 mL (denoted as Sample #02), and 6 mL:2 mL (denoted as Sample #03), in all of which the concentration of each GO and Fe-aminoclay stock solution were 1.7 mg/mL and 1 mg/mL, respectively. After having been let stand for 12 h, precipitation phenomena occurred by means of the self-assembly process due to electrostatic attraction (see Supplementary Information (SI) Fig. S1a). The UV–vis spectra for GO and Fe-aminoclay solution according to each concentration were measured (SI Figs. S2, S3), and the supernatant solution was checked by 200–700 or 800 nm UV–vis spectrophotometry scanning (Optizen 3220UV, Mecasys, Daejeon, Korea) (SI Fig. S1b). Then, after centrifugation at 6000 × *g* for 15 min, the supernatant was removed and the #01, #02, and #03 sample residues were used for dye degradation, the results of which were as follows: 3.4 mg:3 mg (ratio ~1), 6.0 mg:4 mg (ratio ~1.5), and 10.2 mg:2 mg (ratio ~5).

2.4. Fenton-like reaction procedure and analytical method in laboratory

The model organic dyes (MB and OII) were calibrated at 664 nm and 488 nm, respectively (SI Figs. S4, S5). As a preliminary experiment, tests of MB adsorption onto GO and Fe-aminoclay were conducted, whereby 10 mg/L of MB solution with 8.5 μg/mL of GO and 0.25 mg/mL of Fe-aminoclay were prepared using 1000 mg/L of MB stock solution appropriately diluted with DI water. The vials were let stand in a dark room without magnetic stirring.

To investigate dye decoloration by Samples #01, #02, and #03, Fenton-like reactions were performed in 20-mL vials at the temperature of 20 ± 2 °C under minimal light exposure for decoloration of 20 mg/L of MB and OII respectively or a mixture of the two under magnetic stirring, all of which dyes were prepared with DI water. The pH variation was monitored using a pH/ion meter (D-53, Horiba, Kyoto, Japan). All of the experiments were conducted in duplicate with the respective results averaged.

For recycle tests, which entailed recovery of Sample #03, 20 mg/L of MB solution was prepared at 0.5 wt% H_2O_2 concentration, and then 5 runs were repeated after injection of proper MB stock and adjustment with 0.5 wt% H_2O_2 concentration in which interval time of experimental runs is approximately 6 h.

2.5. Characterization of materials used in this study

The morphological observations were made and collected by field-emission transmission electron microscopy (TEM, Tecnai F20 model, Philips Electron Optics, Eindhoven, Netherlands). Samples were prepared by dropping an aliquot of aqueous-solution dispersion onto a carbon-coated copper grid. The excess liquid was absorbed by wiper (Kimtech, Yuhan-Kimberly, Daejeon, Korea). The samples were examined by imaging and elemental analysis using a cold-type field-emission scanning electron microscope (SEM-4700) operable at 0.5–30 V and 1 pA–2 nA, offering resolutions of 1.5 nm at 15 kV or 2.1 nm at 1 kV and magnifications of 20–500,000× range, and equipped with an energy-dispersive X-ray spectrometer (EDX) covering 4Be – 92 U. Atomic force microscopy (AFM) topography images were obtained by means of a NT-MDT AFM in tapping mode at ambient conditions. Raman spectra were measured using a NTEGRA Spectra spectrometer (NT-MDT, Russia) with a spectral resolution of 2 cm^{-1} along with a Cobolt Blues laser (Cobolt, Sweden) operating at a wavelength of 472.8 nm. The measurements were performed at room temperature using a 100× (NA = 0.7) objective with nearly 30 W incident power to avoid sample damage or laser-induced heating. Raman signals were detected by a Newton EMCCD array detector (1600 × 1200 pixels; Peltier cooled to −80 °C), and NT-MDT Nova software was employed for data acquisition and control. The Fourier transform infrared (FT-IR) spectra of the samples (composition: 90 wt% KBr, 10 wt% target materials) were recorded by spectrometry (FT-IR 4100, Jasco, Japan) in the KBr pellet mode. The samples' X-ray diffraction patterns (XRD) were acquired from 3° to 80° with a step size of 0.01 by micro-area X-ray diffractometry (D/MAX-2500, Rigaku, 40 kV and 300 mA), GO film having been prepared by the filtration method using GO solution. Small-angle X-ray scattering (SAXS) data on sample #03 was obtained on a Rigaku (D/MAX-2500, 18 kW), with scan ranging for 0.2–6° of 2θ. N_2 adsorption–desorption isotherms at 77 K for GO powder, Fe-aminoclay, and sample #03 were obtained for provision of the pore parameters including BET (Brunauer, Emmett & Teller) surface area, pore size, and pore volume, using a gas sorption analyzer (NOVA® 4200 Ver. 7.10, USA), after GO powder was prepared by milling of GO films. The size distribution and zeta potential of the samples in aqueous solution was analyzed by dynamic light scattering (DLS) methods (Zetasizer nano zs, Malvern, UK). For the confirmation of free radical detections, DMPO as a spin trapping agent was used for •OH radicals detection [20,41–43]. In the 1-mL Eppendorf tube, 0.1 mL of GO (8.5 μg/mL) solution or Fe-aminoclay solution (2.5 mg/mL) or Sample #01, #02, and #03 was mixed with 0.1 mL of DMPO (0.3 M) in phosphate buffered saline (PBS, 10 mM, pH 7.2), and to this added with 0.1 mL of H_2O_2 (10 mM) in PBS buffer (10 mM, pH 7.2). After 10 min incubation at room temperature, the aliquot of prepared samples transferred into a capillary tube and directly was recorded spectra by electron spin resonance (ESR) spectrometer (JES-FA200, JEOL, Japan). The detailed ESR conditions: center field: 327 mT; power: 1 mW; amplitude: 5.0 × 100; modulation width: 0.4 × 1; sweep width: 1 × 10; sweep time: 30 s. The H_2O_2 concentration of temporal decomposition was measured, following protocol [44]: 2 mL of samples taken was mixed with 0.2 mL of titanium (IV) oxysulfate solution in the 10-mL vials. After 30 s vortexing of them, yellow-colored samples were recorded at 410 nm using UV–vis spectrophotometer.

3. Results and discussion

3.1. Characterization of materials used in this study

Solution-chemistry-based GO was observed by TEM (Fig. 1a and b) and SEM micrography (SI Figs. S6a, S6b). The GO surface morphology showed a few wrinkled sheets as is correspondent with the literature [8,14,40]. In addition, the height of usual GO sheets by an AFM tool was confirmed to approximately 2 nm while flocculated GO with Fe-aminoclay showed uneven heights with a maximum ~40 nm (SI Fig. S7). In contrast, TEM images of organo-building blocks of Fe-aminoclay in aqueous solution (Fig. 1c and d) and SEM images of ethanol-dispersed Fe-aminoclay (SI Figs. S6c, S6d) show stacked layers at the edges of single micro-scale particles. However, the actual size of Fe-aminoclay particles in aqueous solution can be significantly different, owing to the drying of samples dropped onto the grid in TEM sample preparation. Thus, dynamic light scattering (DLS) analysis of the hydrodynamic diameter of Fe-aminoclay (2.5 mg/mL) in aqueous solution therefore could provide a more exact size distribution, which in the present case was ~93.2 nm with particle size index (0.562), presenting that the predominant size of Fe-aminoclay is distributed in nanoscale level. For Sample #03, which was self-assembled (i.e., flocculated as a heterogeneous catalyst in a Fenton-like reaction), Fig. 1e and f shows a large proportion of the GO surface covered with Fe-aminoclay. Detailed SEM images of sample #03 (Fig. 2) in fact show the Fe-aminoclay densely sheathed onto the GO surface. Elemental energy-dispersive X-ray spectroscopic (EDX) maps of C, Fe, and Cl (Fig. 2e) in which Cl^- ions exist as stabilized ions for positively charged $-NH_3^+$ groups of Fe-aminoclay, verify the homogeneous coating of Fe-aminoclay over the entire GO surface. Interestingly, the density of the Fe element is higher on the wrinkled surface of the GO sheets (Fig. 2e inset). This is a similar pattern in the previous reports [45,46] like the immobilization of oxidase enzyme onto GO surfaces as an artificial enzyme mimicking system. It is noted that for the microscopic images of Samples #01 and #02, compared to that of Sample #03, we could not find any discrete difference. Thus, morphological observation was concentrated on Sample #03, not both Samples #01 and #02.

In order to investigate the impurities and analyze the structure of the as-prepared materials, their XRD patterns were examined (SI Fig. S8). The characteristics peaks of Fe-aminoclay are confirmed in SI Fig. S8a: the broad in-plane reflections at 2θ = 6.12°, 11.66°, 22.76°, 35.15°, and 60.89° correspond to d_{001} = 14.49 Å, d_{002} = 7.56 Å, $d_{020,110}$ = 3.90 Å, $d_{130,200}$ = 2.55 Å, and $d_{060,330}$ = 1.52 Å. The basal spacing of d_{001} indicates a regular layer structure. Based on the intra-plane reflections, especially the very weak reflection at $d_{060,330}$, which is slightly different

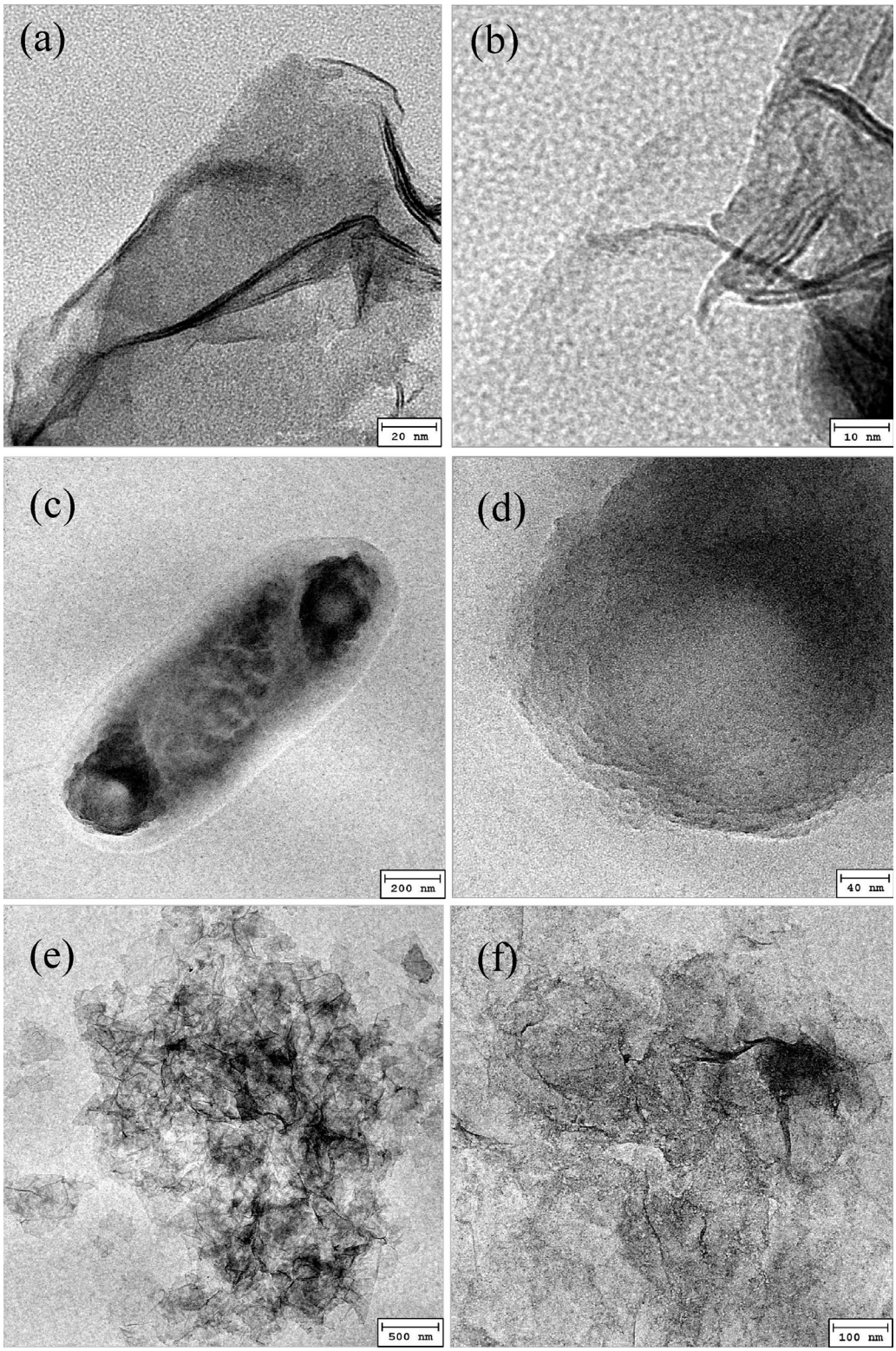

Fig. 1. Transmission electron microscope (TEM) images of GO sheets (a and b), organo-building blocks of Fe-aminoclay (c and d), and Sample #03 (e and f) in aqueous solution.

for talc-like 2:1 trioctahedral phyllosilicate of 3-aminopropyl functionalized magnesium phyllosilicate, the Fe-aminoclay was close to amorphous (poor crystalline phase) 1:1 dioctahedral phyllosilicate [26]. In the case of the GO film (paper), it had a distinct peak at 10.89° (as calculated by Bragg equation), corresponding to a d-spacing of 8.12 Å, while the graphite peak occurred at >2θ = 25°, indicating that the interlayer spacing of the GO film had increased due to the presence of water molecules between the sheet's layers [8,40] and a broad shoulder peak appeared at 2θ = 18.70. When it was checked the XRD peaks of graphite powder at 2θ = 3–35°, it was not observed any related peaks (data not shown). The reflection peaks of self-assembled sample #03 at 2θ = 10.87°, 18.04°, and

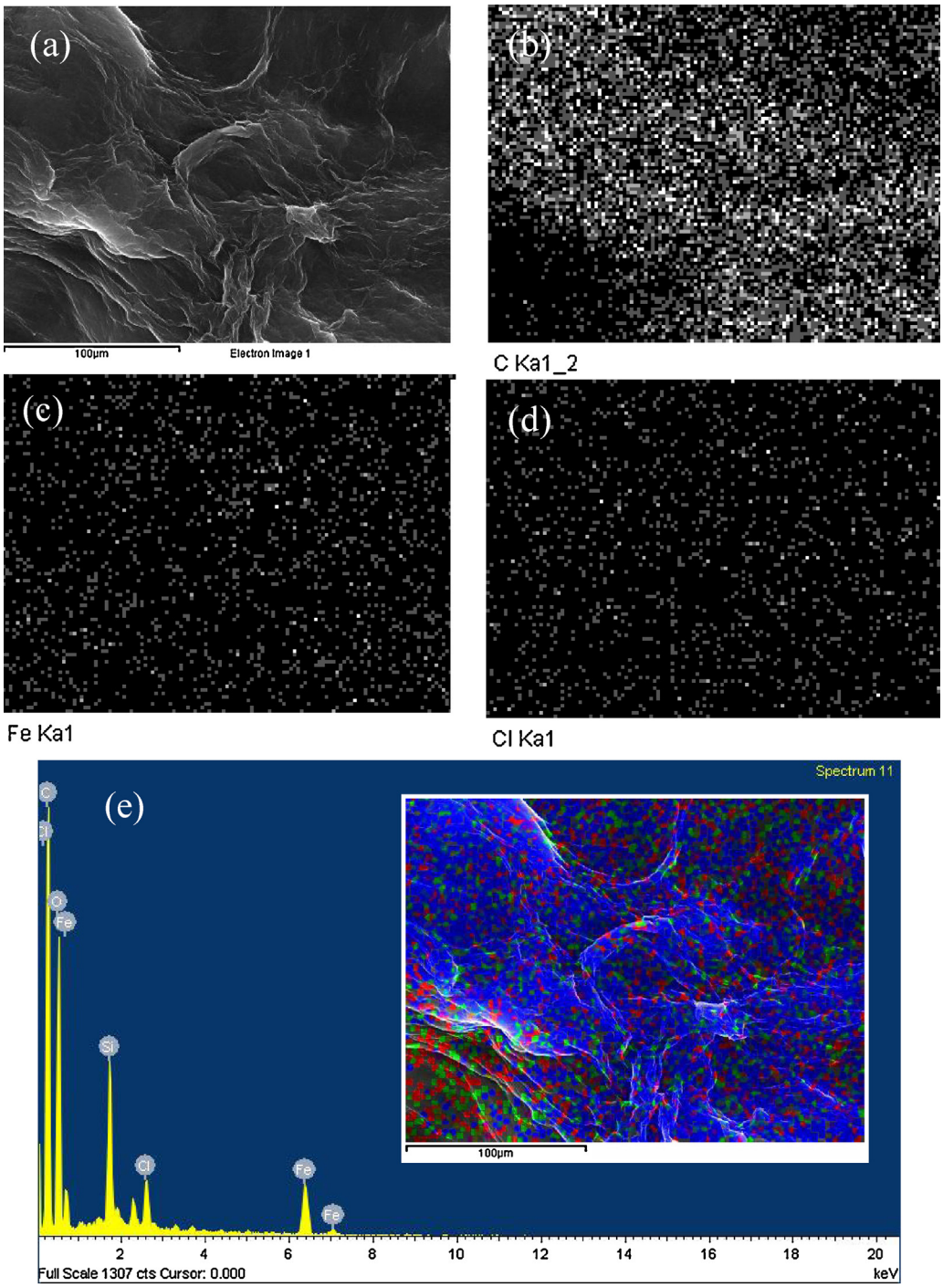

Fig. 2. Scanning electron microscopic (SEM) micrographs of Sample #03 (a) as well as C (b, blue), Fe (c, red), and Cl (d, green) by elemental mapping, and energy-dispersive X-ray (EDX) microanalysis (e) whose inset shows merged images (from b to d). (For interpretation of the references to color in this figure legend, the reader is referred to the web version of the article.)

23.25° were correspondent with d_{002} = 8.12 Å, $d_{020,110}$ = 4.93 Å, and $d_{130,200}$ = 3.82 Å. The spacing distances of the fundamental in-plane reflection peaks were slightly increased relative to pure Fe-aminoclay powder, but were not significantly changed, as reflected the fact that the self-assembled materials had retained their intrinsic clay structures. In order to confirm the mesolamellar structure of Sample #03, small-angle X-ray scattering (SAXS) data were obtained, but no intensive peaks were observed (SI Fig. S9).

Fig. 3 shows FT-IR spectra that confirm the materials' organo-functionalities. The organic entities of Fe-aminoclay was suggested as $-(CH_2)_3-NH_2$ by covalent linking to Fe metals, consisting of water-solubilized Fe-based aminoclay in the organic–inorganic hybrid-type organoclay family [9,26,47]. The peaks of GO at <900 cm^{-1} can be disregarded, as they are overly complex structural signals [48]. Interestingly, in self-assembled Sample #03 the vibration of the H_2O and —OH groups in the GO peaks disappeared, indicating that, along with the interaction of the hydroxyl groups with the peak shifts, the Fe-aminoclay particles had strongly interacted with the carbonyl/carboxylic and ester groups of GO. Hence, the resultant peaks of Sample #03, as displayed: the —OH groups

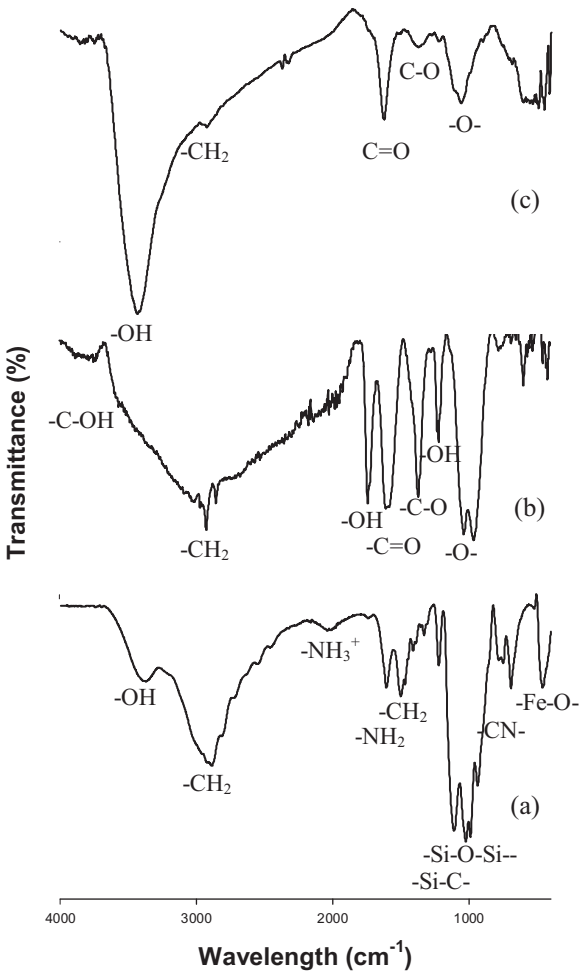

Fig. 3. Fourier transform infrared (FT-IR) spectra of Fe-aminoclay powder (a), GO film (b), and Sample #03 (c).

at 3409 cm^{-1}, the —CH_2 groups at 2910 cm^{-1}, the H_2O groups at 1622 cm^{-1}, the deformation of the —OH groups at 1342 cm^{-1}, and the epoxy (—O—) groups at 1044 cm^{-1}. Thus, the Fe-aminoclay was more densely decorated at the edge than the basal on the GO surface. Moreover, this could reasonably be inferred from the mapping image (Fig. 2e inset).

The Raman spectra of the GO and Sample #03 after five consecutive runs were checked with reference to the D and G bands at 1600 cm^{-1} and 1356 cm^{-1}, respectively (SI Fig. S10). The D band was related to the defects of the hydroxyl and epoxide groups in the in-plane sp^2-conjugated carbon structure of GO [8,40]. The D/G intensity ratio of GO was similar to that of Sample #03 after the five consecutive runs. The slight shift of the D bands of GO and Sample #03, from 1359 to 1363 cm^{-1}, was evidence of a specific interaction of GO and Fe-aminoclay. Importantly, after several recycles of Sample #03, the intrinsic GO materials, in combination with the positively charged aminoclays, could be a suitable catalyst for the heterogeneous Fenton-like reaction.

In order to check the surface charge potential of catalysts in aqueous solution, zeta potential values were measured (SI Fig. S11), showing ~−30.77 and ~+35.57 mV for respective GO (8.5 μg/mL) and Fe-aminoclay (2.5 mg/mL) and ~−10.34, ~+16.63, and ~+31.87 mV for Sample #01, #02, and #03 as increase in Fe-aminoclay dosage.

3.2. Preliminary test of H_2O_2 decomposition by each GO and Fe-aminoclay for MB decoloration

In order to examine H_2O_2 decomposition by each water-soluble GO and Fe-aminoclay as a means of generating free radicals for degradation of organic matter, 10 mg/L of MB as a recalcitrant dye was selected for decoloration by GO at 8 μg/mL and by Fe-aminoclay at 0.25 mg/mL, as monitored at near-neutral pH according to the H_2O_2 concentration (Fig. 4). As the H_2O_2 concentration in the Fe-aminoclay in 10 mg/L of MB solution was increased, the decoloration rate was gradually improved. Due to the electrostatic repulsion between the positively charged organo-building blocks of Fe-aminoclay and the cationic MB molecules, adsorption of MB onto the Fe-aminoclay was negligible. In the case of no H_2O_2 injection, MB was not degraded for seven days. However, >0.5 wt% H_2O_2, at a loading of 0.25 mg/mL of Fe-aminoclay, achieved ~100% decoloration after seven days (Fig. 4a). By contrast, negatively charged GO with carboxyl and hydroxyl groups interacted with MB molecules and immediately precipitated due to the blocking of negatively charged sites by electrostatic attraction or the π–π interaction resulting from contact with aromatic carbon structures [49], as confirmed by the shift of the MB absorbance peak in the presence of GO (SI Fig. S12), which was observed with the naked eye (Fig. 4b). Notably, the precipitate, MB, which adsorbed GO after flowing out of the supernatant, was injected with 0.5 wt% of H_2O_2 after seven days, and the GO was perfectly restored to its brown color and original water-soluble condition. After adding MB stock solution to GO solution, which produced 10 mg/L of MB, the samples were let stand for one day in a dark room to enable full adsorption of MB onto GO. Approximately half of the MB molecules were adsorbed onto the GO, showing an adsorption capacity of GO for MB of 0.0566 mg MB/μg GO. The adsorption kinetics showed that within the initial 30 min, most of MB molecules had adsorbed, attaining thereby an asymptotic curve (data not shown). Also, as the H_2O_2 concentration was from 0% to 3.0 wt%, the degradation rate was enhanced (Fig. 4c). In the control, without H_2O_2 treatment, the degradation of MB was minimal for the results of another control experiment, this one set up to observe the H_2O_2 effect without all GO and Fe-aminoclay, showed that autocatalysis of unstable H_2O_2 by association or decomposition caused MB decoloration (Fig. 4d) [34,50]. 1.0 wt% H_2O_2 treatment demonstrated the best removal efficiency, about 50% for 3.0 wt% H_2O_2 treatment case. It is associated with excess H_2O_2 acted radical scavenging for •OH radicals, producing H_2O and •OOH radicals [35,38]. Consequently, based on the control findings for both no H_2O_2 treatment in GO or Fe-aminoclay and only H_2O_2 treatment without catalysts, each GO and Fe-aminoclay played a role in the H_2O_2 decomposition generating •OH radicals. Oxygenated groups of water-soluble GO [18] or Fe atoms of Fe-aminoclay [26] under near-neutral pH conditions can decompose H_2O_2 molecules to produce •OH radicals for degradation of aromatic carbon structures (SI Fig. S13, S14). Both GO and Fe-aminoclay in the presence of H_2O_2 produced •OH radicals (SI Fig. S15). Particularly the intensity of ESR peaks was increased from Sample #01 to Sample #03. This is related to fast dye decoloration of Sample #03. In fact, GO and Fe-aminoclay are generating both •OH radicals [20,27] and •OOH radicals [7,26] because those materials are based on Fenton-like reaction ($Fe^{3+} + H_2O_2 \rightarrow$ •OOH + $H^+ + Fe^{2+}$). Peroxidase mechanism system of GO [7] and Fe-aminoclay [26] in the presence of H_2O_2 as biosensor applications were demonstrated. Therefore, the predominant removal mechanism of dyes is considered to be •OH radicals than •OOH radicals because •OH radicals is more strongly non-selective attackers to break aromatic structure of dyes, corresponding to results of decrease in H_2O_2 concentration. According to temporal H_2O_2 concentration at 20 mg/L of MB solution after 0.01 wt% H_2O_2 treatment (SI Fig. S16), the H_2O_2 concentration was decreased gradually while H_2O_2 concentration was

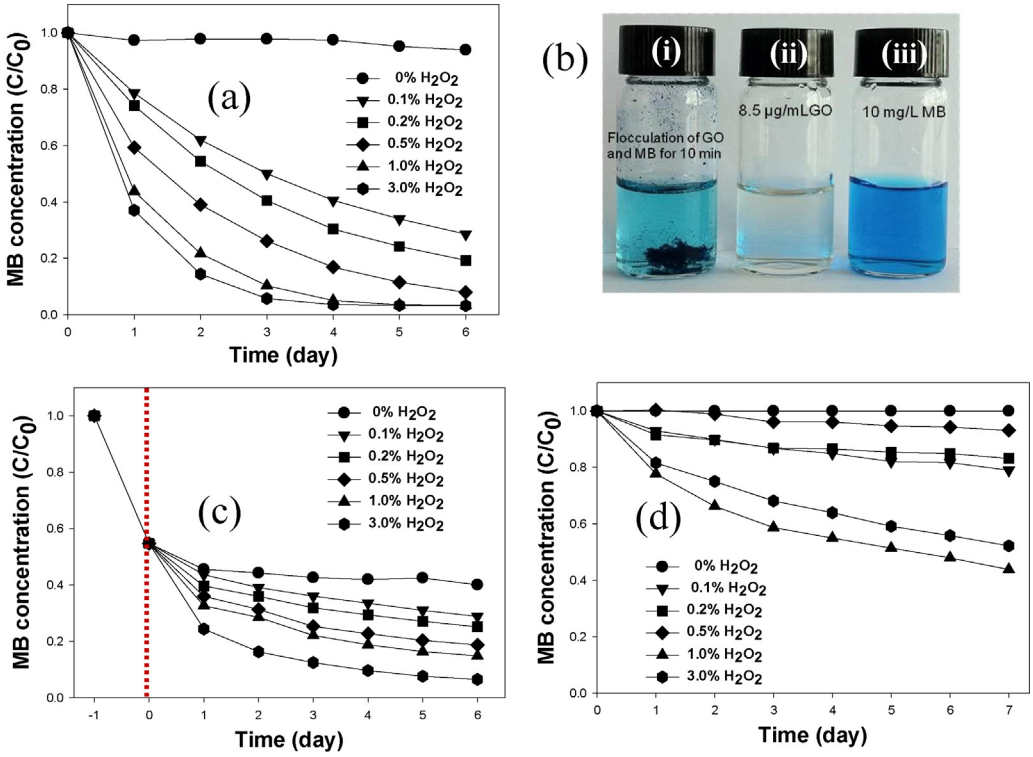

Fig. 4. Fenton-like reaction of Fe-aminoclay (0.25 mg/mL) (a) according to H_2O_2 concentration at pH 6.5 and 20 ± 2 °C, dica-camera image (b) of flocculated GO by MB molecules (I), dispersed 8.5 μg/mL of GO (II) in aqueous solution, and 10 mg/L of MB (III) in aqueous solution. Fenton-like reaction of GO (8.5 μg/mL) (c) in which dotted brown line indicates the time of H_2O_2 introduction after MB adsorption for one day and no-catalysts as the control (d) according to H_2O_2 concentration at pH 6.0 and 20 ± 2 °C.

relatively less reduced in the absence of catalysts. In addition, at a neutral pH, the Fe(IV) species, as a non-radical system, cannot effectively break the ring structure of organic matter [22], because it is more weakly attacking radicals compared with •OH radicals.

3.3. MB or OII dye decoloration by self-assembled Samples #01, #02, and #03 according to H_2O_2 loading

Figs. 5 and 6 show the decoloration of 20 mg/L of each MB and OII by Samples #01, #02, and #03 in the presence of various H_2O_2 concentrations (1.0 wt%, 0.5 wt%, 0.1 wt%, and 0.01 wt%) at pH 6.0 after dye adsorption for one hour. Upon visual inspection, MB on Samples #01, #02, and #03 after 6 h for 1.0 wt% H_2O_2 treatment was clearly observed (SI Fig. S14). In all cases, and in both in MB and OII solutions, the decoloration rate was enhanced as the H_2O_2 concentration and sample number were increased. As a result, the Sample #03 catalyst (12.2 mg) presented the best performance in all of the cases, while the 1.0 wt% and 0.5 wt% H_2O_2 treatments achieved ~100% decoloration at 4 h and 5 h, respectively, for MB degradation. After the 1 h adsorption period (SI Fig. S17), the patterns of OII degradation showed a similar trend but ~100% decoloration was achieved within 2 h for the 1.0 wt% and 0.5 wt% H_2O_2 treatments (Fig. 6a and b). Faster degradation of OII than of MB is related not only to molecular structure but also the easy interaction of positively charged Fe-aminoclay particles on the GO surface. However, it might be less effective for the initial dye adsorption capacity. The pH values slightly fluctuated, decreasing about 0.3 unit of pH after 5 h reaction, due to the formation of intermediates (data not shown) [38]. The apparent discoloration kinetics of MB and OII in solution can be expressed by the pseudo first-order equation [50].

$$r = -\frac{dC}{dt} = k_a C,$$

where r is the reaction rate, C is the concentration of dye in aqueous solution, t is the reaction time, and k_a is the pseudo first-order rate constant. The plot of $-\mathrm{Ln}(C/C_0)$ as a function of reaction time t led, with linear regression, to the k_a constants by the slopes of the straight line. The obtained rate constants for Figs. 5 and 6 are listed in Table 1 for MB and OII removal. Under conditions below 0.1 wt% of H_2O_2 (Fig. 6c and d), the deviation from the straight line became significant, indicating that the results were less reliable. For the reaction constants compared other dye degradation rates [51,52], the low rate constant, approximately one order of magnitude lower than that in other studies of the literature, could be attributed to the low loading of the catalyst as well as the decrease in the surface area and pore size, attributable to the self-assembly process, that limited the access to dye molecules (SI Table S1). Thus, in order to enhance reaction rates and treatment capacity, increases both in catalyst loading and in controlled porosity as a filler in scale-up packing column experiments, along with total organic carbon (TOC) monitoring, will be undertaken in upcoming research.

3.4. Decoloration of MB and OII mixture by Samples #01, #02, and #03

To determine the treatment feasibility of cationic and anionic dyes as a mixture solution prior to investigating the adsorption phenomena (SI Fig. S18), 20 mg/L of MB and OII mixture solution was simultaneously treated by Samples #01, #02, and #03 (SI Fig. S19). Based on Figs. 5b and 6b, the concentration of 0.5 wt% H_2O_2 for 20 mg/L of MB and OII mixture treatment is considered to be an optimal condition for a Fenton-like system following the same protocol as outlined above. Interestingly, in all of the cases, MB was more quickly degraded that OII within the same reaction time. This is unexpected given the OII degradation shown in Fig. 6. The accessibility of MB molecules to Samples #01, #02, and #03 might

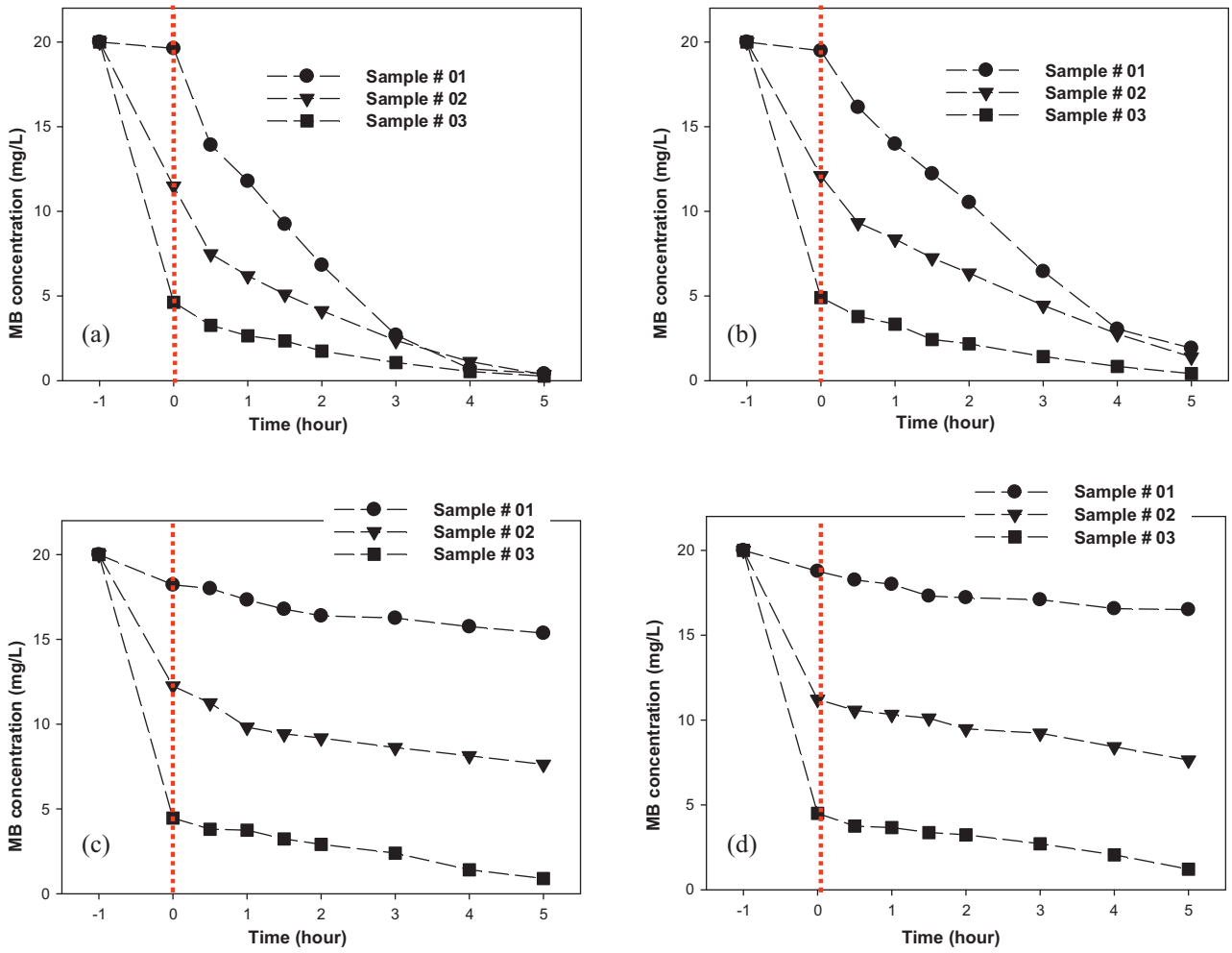

Fig. 5. Decoloration of 20 mg/L of MB solution by self-assembled GO with organo-building blocks of Fe-aminoclay (Samples #01, #02, and #03) according to H_2O_2 concentration at pH 6.0 and 20 ± 2 °C; 1.0 wt% H_2O_2 treatment (a), 0.5 wt% H_2O_2 treatment (b), 0.1 wt% H_2O_2 treatment (c), and 0.01 wt% H_2O_2 treatment (d). Note that the dotted brown lines indicate the time of H_2O_2 introduction after one-hour adsorption of MB. (For interpretation of the references to color in this figure legend, the reader is referred to the web version of the article.)

assist MB molecules' contact with the GO surface due to hydrophobic or π–π interactions. As shown in zeta potential values (SI Fig. S11), GO with negative charges easily interacted with cationic dye molecules, facilitating degradation of those dyes fast while Fe-aminoclay with positive charges facilely adsorbed with anionic dye molecules, resulting in degradation of those dyes in the presence of H_2O_2. In case of Samples #01, #02, and #03, zeta potential values were increased as increase in Fe-aminoclay dosage. As a result, decoloration of MB was faster than that of OII in both Sample #01 and #02, but the discrepancy of decoloration rate for MB and OII in Sample #03 was negligible. Probably, it is associated with electrostatic interactions because the degradation phenomena of dyes occur predominantly on (near) surface of catalyst materials.

Five-time consecutive recycles of Sample #03 resulted in no loss of catalyst activity with similar degradation patterns (SI Fig. S20), indicating that this catalyst can be used in the scale-up systems with a continuous operation.

In summary, self-assembled GO with organo-building blocks of Fe-aminoclay could be a suitable catalyst for removal of differently charged organic matter in a heterogeneous Fenton-like reaction at

Table 1
Pseudo first-order rate constants for decoloration of MB and OII.

H_2O_2 loading	k_a, h^{-1} for MB	r^2	k_a, h^{-1} for OII	r^2
1.0 wt% (Sample #01, 0.32 mg/mL)	0.23938	0.9883	0.56852	0.9701
1.0 wt% (Sample #02, 0.50 mg/mL)	0.27764	0.9677	0.52967	0.9480
1.0 wt% (Sample #03, 0.61 mg/mL)	0.35288	0.9721	0.57930	0.9581
0.5 wt% (Sample #01, 0.32 mg/mL)	0.20496	0.9868	0.59543	0.9746
0.5 wt% (Sample #02, 0.50 mg/mL)	0.17522	0.9721	0.68002	0.9603
0.5 wt% (Sample #03, 0.61 mg/mL)	0.20433	0.9745	0.62333	0.9724
0.1 wt% (Sample #01, 0.32 mg/mL)	0.13393	0.9534	0.05929	0.8325
0.1 wt% (Sample #02, 0.50 mg/mL)	0.03756	0.9052	0.14734	0.9878
0.1 wt% (Sample #03, 0.61 mg/mL)	0.01465	0.9383	0.23798	0.9801
0.01 wt% (Sample #01, 0.32 g/mL)	0.10004	0.9257	0.01575	0.9406
0.01 wt% (Sample #02, 0.50 g/mL)	0.03123	0.9833	0.02124	0.6760
0.01 wt% (Sample #03, 0.61 g/mL)	0.01078	0.8930	0.01199	0.7491

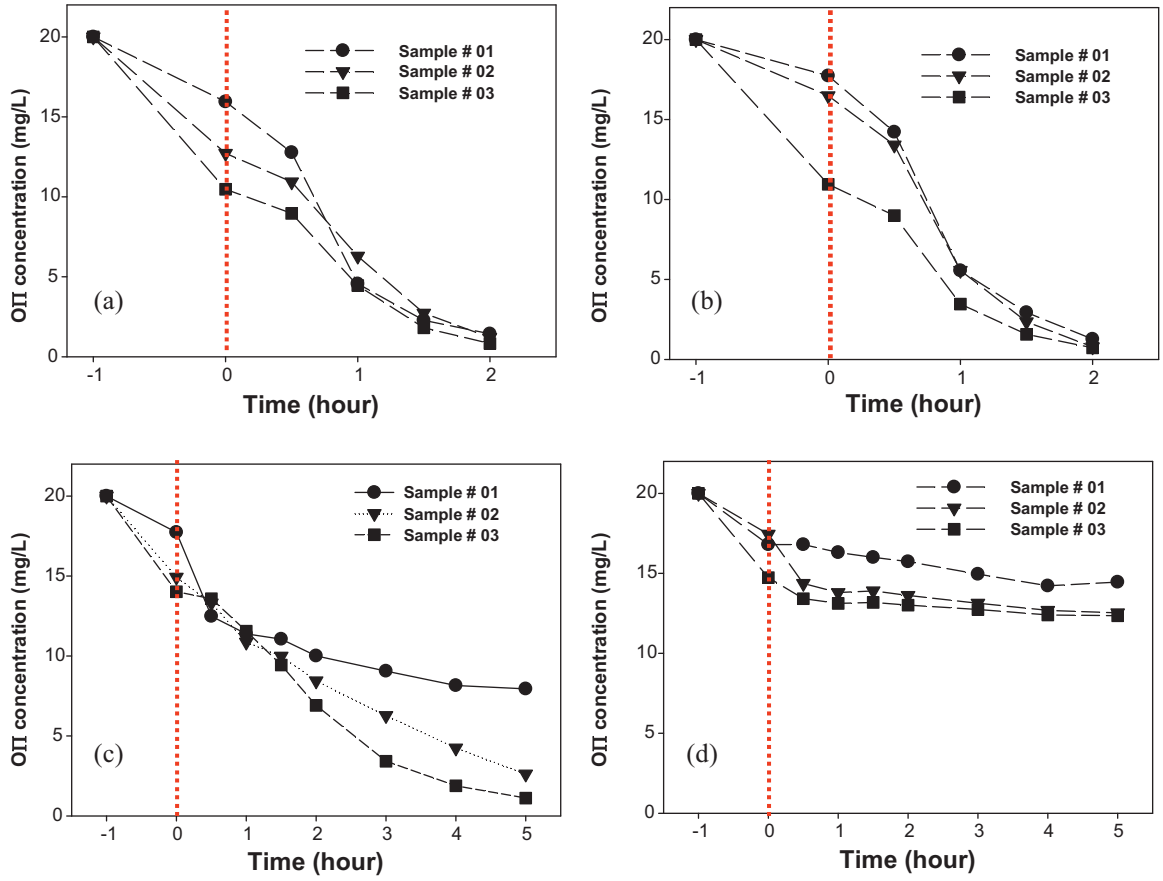

Fig. 6. Degradation of OII solution by self-assembled GO with organo-building blocks of Fe-aminoclay (Samples #01, #02, and #03) according to H_2O_2 concentration at pH 6.0 and 20 ± 2 °C; 1.0 wt% H_2O_2 treatment (a), 0.5 wt% H_2O_2 treatment (b), 0.1 wt% H_2O_2 treatment (c), and 0.01 wt% H_2O_2 treatment (d). Note that the dotted brown lines indicate the time of H_2O_2 introduction after one-hour adsorption of OII. (For interpretation of the references to color in this figure legend, the reader is referred to the web version of the article.)

neutral pH. Additionally, the effects on other, coexisting ions and ubiquitous humic acid should be studied.

4. Conclusion

The operation conditions at neutral pH, as a heterogeneous catalysis system for water and wastewater treatment, are essential to advanced oxidation processes (AOP). Because the iron salt-based homogeneous Fenton reaction usually shows best activity at pH 3, pH adjustment prior to and after treatment is required, which produces residual sludge [53]. Operation under neutral pH conditions, contrastingly, does not require pH control. A heterogeneous catalyst system, additionally, does not produce sludge, and because it can recycle processes, catalyst costs can be reduced. Significantly, both GO and Fe-aminoclay are not in ionic form but rather are water-soluble particles, indicating that that the heterogeneous system in fact functions as a homogeneous system. However, those materials, due to their water-soluble property, have to be immobilized onto a macro-sized matrix [54]. In shown in this study, the self-assembled precipitation method can be an effective approach for overcoming the challenges of Fenton-like reactions.

Acknowledgements

This research was supported by the General Research Project of the Korea Institute of Geoscience and Mineral Resources funded by the Ministry of Knowledge Economy of Korea to T. Ryu. We also acknowledge the financial support by National Research Foundation of Korea (NRF) funded by the Ministry of Education, Science and Technology (#2012R1A1B4002413) and Inha University. The authors are indebted to Jane Chung for the graphical abstract.

Appendix A. Supplementary data

Supplementary data associated with this article can be found, in the online version, at http://dx.doi.org/10.1016/j.apcatb.2013.05.066.

References

[1] S. Mann, Nature Materials 8 (2009) 781–792.
[2] A.J. Patil, S. Mann, Journal of Materials Chemistry 18 (2008) 4605–4615.
[3] S.I. Stupp, P.V. Braun, Science 277 (1997) 1242–1248.
[4] D.I. Rożkiewicz, B.D. Myers, S.I. Stupp, Angewandte Chemie International Edition 50 (2011) 1–5.
[5] A.J. Patil, J.L. Vickery, T.B. Scott, S. Mann, Advanced Materials 21 (2009) 1–6.
[6] S. Mann, Angewandte Chemie International Edition 47 (2008) 5306–5320.
[7] Y. Song, W. Wei, X. Qu, Advanced Materials 23 (2011) 4215–4236.
[8] B.G. Choi, H. Park, T.J. Park, M. Yang, J.S. Kim, S.-Y. Jang, N.S. Heo, S.Y. Lee, J. Kong, W.H. Hong, ACS Nano 4 (2010) 2910–2918.
[9] Y.-C. Lee, E.J. Kim, D.A. Ko, J.-W. Yang, Journal of Hazardous Materials 196 (2011) 101–108.
[10] F. Caruso, R.A. Caruso, H. Möhwald, Science 282 (1998) 1111–1113.
[11] P. Chaturbedy, D. Jagadeesan, M. Eswaramoorthy, ACS Nano 4 (2010) 5921–5929.
[12] W.S. Hummers, R.E. Offeman, Journal of the American Chemical Society 80 (1958) 1339.
[13] D. Chen, H. Feng, J. Li, Chemical Reviews 112 (2012) 6027–6053.
[14] Y.-C. Lee, J.-W. Yang, Journal of Industrial and Engineering Chemistry 18 (2012) 1178–1185.
[15] T.S. Sreeprasad, S.M. Maliyekkal, K.P. Lisha, T. Pradeep, Journal of Hazardous Materials 186 (2011) 921–931.

[16] X. Zhang, C. Cheng, J. Zhao, L. Ma, S. Sun, C. Zhao, Chemical Engineering Journal 215–216 (2013) 72–81.
[17] Y. Gao, Y. Li, L. Zhang, H. Huang, J. Hu, S.M. Shah, X. Su, Journal of Colloid and Interface Science 368 (2012) 540–546.
[18] Y. Song, K. Qu, C. Zhao, J. Ren, X. Qu, Advanced Materials 22 (2010) 2206–2210.
[19] L. Gao, J. Zhuang, L. Nie, J. Zhang, Y. Zhang, N. Gu, T. Wang, J. Feng, D. Yang, S. Perrett, X. Yan, Nature Nanotechnology 2 (2007) 577–583.
[20] W. Zhang, C. Wang, Z. Li, Z. Lu, Y. Li, J.-J. Yin, Y.-T. Zhou, X. Gao, Y. Fang, G. Nie, Y. Zhao, Advanced Materials 24 (2012) 5391–5397.
[21] J. Zhang, J. Zhuang, L. Gao, Y. Zhang, N. Gu, J. Feng, D. Yang, J. Zhu, X. Yan, Chemosphere 73 (2008) 1524–1528.
[22] A. Le-Tuan Pham, C. Lee, F.M. Doyle, D.L. Sedlak, Environmental Science and Technology 43 (2009) 8930–8935.
[23] R. Gonzalez-Olmos, M.J. Martin, A. Georgi, F.-D. Kopinke, I. Oller, S. Malato, Applied Catalysis B: Environmental 125 (2012) 51–58.
[24] C.-L. Hsueh, Y.-H. Huang, C.-C. Wang, C.-Y. Chen, Journal of Molecular Catalysis A: Chemical 245 (2006) 78–86.
[25] S. Wang, Dyes and Pigments 76 (2008) 714–720.
[26] Y.-C. Lee, M.I. Kim, M.-A. Woo, H.G. Park, J.-I. Han, Biosensors and Bioelectronics 42 (2013) 373–378.
[27] Y.-C. Lee, Y.S. Huh, W. Farooq, J.-I. Han, Y.-K. Oh, J.-Y. Park, RSC Advances (2013), http://dx.doi.org/10.1039/C3RA23266B (submitted for publication).
[28] A.J. Patil, M. Li, E. Dujardin, S. Mann, Nano Letters 7 (2007) 2660–2665.
[29] Y.-C. Lee, E.J. Kim, J.-W. Yang, H.-J. Shin, Journal of Hazardous Materials 192 (2011) 62–70.
[30] H.-K. Han, Y.-C. Lee, M.-Y. Lee, A.J. Patil, H.-J. Shin, ACS Applied Materials & Interfaces 3 (2011) 2564–2572.
[31] Y.-C. Lee, E.S. Jin, S.W. Jung, Y.-M. Kim, K.S. Chang, J.-W. Yang, S.-W. Kim, Y.-O. Kim, H.-J. Shin, Scientific Reports 3 (2013) 1292 (1–8).
[32] A.W. Vermilyea, B.M. Voelker, Environmental Science and Technology 43 (2009) 6927–6933.
[33] S.H. Tian, Y.T. Tu, D.S. Chen, X. Chen, Y. Xiong, Chemical Engineering Journal 169 (2011) 31–37.
[34] S. Yang, H. He, D. Wu, D. Chen, Y. Ma, X. Li, J. Zhu, P. Yuan, Industrial and Engineering Chemistry Research 48 (2009) 9915–9921.
[35] Z. Ai, L. Lu, J. Li, L. Zhang, J. Qiu, M. Wu, Journal of Physical Chemistry C 111 (2007) 7430–7436.
[36] M.F. Variava, T.L. Church, A.T. Harris, Applied Catalysis B: Environmental 123–124 (2012) 200–207.
[37] C. Fan, L. Tsui, M.-C. Liao, Chemosphere 82 (2011) 229–236.
[38] J. Shin, Y.-C. Lee, Y. Ahn, J.-W. Yang, Desalination and Water Treatment 50 (2012) 102–114.
[39] G.P. Kotchey, B.L. Allen, H. Vedala, N. Yanamala, A.A. Kapralov, Y.Y. Tyurina, J. Klein-Seetharaman, V.E. Kagan, A. Star, ACS Nano 5 (2011) 2098–2108.
[40] B.G. Choi, M. Yang, W.H. Hong, J.W. Choi, Y.S. Huh, ACS Nano 6 (2012) 4020–4028.
[41] L. Yan, F. Zhao, S. Li, Z. Hu, Y. Zhao, Nanoscale 3 (2011) 362–382.
[42] R.J. Elias, M.L. Andersen, L.H. Skibsted, A.L. Waterhouse, Journal of Agricultural and Food Chemistry (2013), http://dx.doi.org/10.1021/jf8035484.
[43] J.-J. Yin, F. Lao, P.P. Fu, W.G. Wamer, Y. Zhao, P.C. Wang, Y. Qiu, B. Sun, G. Xing, J. Dong, X.-J. Liang, C. Chen, Biomaterials 30 (2009) 611–621.
[44] E. Isarain-Chávez, C. de la Rosa, C.A. Martínez-Huitle, J.M. Peralta-Hernández, International Journal of Electrochemical Science 8 (2013) 3084–3094.
[45] Y. Guo, L. Deng, J. Li, S. Guo, E. Wang, S. Dong, ACS Nano 5 (2011) 1282–1290.
[46] Y. Liu, D. Yu, C. Zeng, Z. Miao, L. Dai, Langmuir 26 (2010) 6158–6160.
[47] A. Bagri, C. Mattevi, M. Acik, Y.J. Chabal, M. Chhowalla, V.B. Shenoy, Nature Chemistry 2 (2010) 581–587.
[48] D.W. Lee, V.L.D.L. Santos, J.W. Seo, L.L. Felix, D.A. Bustmante, J.M. Cole, C.H.W. Barnes, Journal of Physical Chemistry B 114 (2010) 5723–5728.
[49] D. Wang, Y. Li, P. Hasin, Y. Wu, Nano Research 4 (2011) 124–130.
[50] J. Feng, X. Hu, P.L. Yue, Water Research 40 (2006) 641–646.
[51] S.S. Gupta, M. Stadler, C.A. Noser, A. Ghosh, B. Steinhoff, D. Lenoir, C.P. Horwitz, K.-W. Schramm, T.J. Collins, Science 296 (2002) 326–328.
[52] Y. Huang, J. Li, W. Ma, M. Cheng, J. Zhao, J.C. Yu, Journal of Physical Chemistry B 108 (2004) 7263–7270.
[53] X. Yang, P.-F. Tian, C. Zhang, Y.-q. Deng, J. Xu, J. Gong, Y.-F. Han, Applied Catalysis B: Environmental 134–135 (2013) 145–152.
[54] N. Ferroudj, J. Nzimoto, A. Davidson, D. Talbot, E. Briot, V. Dupuis, A. Bée, M.S. Medjram, S. Abramson, Applied Catalysis B: Environmental 136–137 (2013) 9–18.